# Soft Matter

Accepted Manuscript






ROYAL SOCIETY OF CHEMISTRY

www.rsc.org/softmatter

# Freely drawn single lipid nanotube patterns

*Kaori Sugihara,* Amin Rustom and Joachim P. Spatz*

Max Planck Institute for Intelligent Systems, Dept. New Materials and Biosystems & University of Heidelberg, Institute for Physical Chemistry, Dept. Biophysical Chemistry; postal address: Heisenbergstr. 3, 70569 Stuttgart, Germany

* corresponding author: kaori.sugihara@unige.ch



**Abstract**

LNTs are unique 3D structures made only of safe and abundant biomaterials by self-assembly. Current bottleneck for developing applications using LNTs is lack of easy technique to pattern them on substrates. We report a method to free draw single lipid nanotube (LNT) patterns in any shape on surfaces with 1,2-dioleoyl-sn-glycero-3-phosphoethanolamine (DOPE) that takes inverted hexagonal ($H_{II}$) phase. We used pre-self-assembled LNTs or $H_{II}$ lipid blocks as a lipid reservoir from which new LNTs were pulled by applying a point load with a micromanipulator. The extreme simplicity of our technique originates from the fundamental nature of DOPE lipids that prefer $H_{II}$ phase, while all the conventional approaches use PC lipids that from lamellar phase. By adjusting the surface properties with polyelectrolyte multilayers, the created single LNT objects are able to stay adhered to the surface for over a week. Importantly, it could be shown that two vesicles loaded with caged fluorescent molecules were able to fuse well with a LNT, enabling diffusive transport of uncaged fluorescent molecules from one vesicle to the other.

## Introduction

Single lipid nanotubes (LNTs) self-assemble in solution, induced by lipid phase transition.[1-3] They are unique 3D structures made only of safe and abundant biomaterials by self-assembly. Such nano-materials inspired by biological systems have a potential in future nanotechnology. For example, Schnur and coworkers used the LNTs as a template to create metal nanotubes by electroless-metallization techniques.[4] They have made a further effort to create products using those metal nanotubes such as a cathode for vacuum field emission and capsules for controlled drug release.[4] Although the work presented is an excellent example of possible use of lipids in engineering, the applications using these LNTs were still limited because the LNT templates are floating in solution. Therefore, assembling and additional patterning of LNTs on surfaces is the next key step to develop broader synthetic nanotechnology systems.[5-8] The first controlled single LNT patterning was reported in Nature in 2001 by Orwar Group.[9] Their technique is based on the fission of surface-immobilized GUVs by micromanipulation and voltage pulse application. The approach spans LNTs with a diameter of 200 – 400 nm between GUVs, producing LNT-GUV networks. As an alternative approach, Shimizu Group reported the construction of LNT objects by picking and placing individual LNTs on surfaces with a micromanipulator.[5] The elimination of the voltage application was a great simplification in the experimental setup. However, the created objects were made of several LNTs thus were disconnected each other.

Previously, we have reported that 1,2-dioleoyl-sn-glycero-3-phosphoethanolamine (DOPE) lipid blocks adsorbed on a polyelectrolyte-functionalized surface transformed their shape into single-bilayer-wall tubes upon the application of solution flow.[10] DOPE is a zwitterionic conically shaped lipid. It has garnered attention due to its inverted hexagonal phase ($H_{II}$).[11-13] In aqueous solution at room temperature, it forms $H_{II}$ blocks, frequently characterized by cryo-electron microscopy.[14, 15] The $H_{II}$ lipid blocks adsorbed on glass

surfaces coated by cationic polyelectrolytes such as polyethylenimine (PEI) and polylysine (PLL). Upon solution flow, the lipid blocks move while a part of the block is attached to the substrate, thus protruding LNTs. Independent of the strength of the solution flow, the diameter of the LNTs stabilizes at 19.1 ± 4.5 nm, confirmed by cryo-transmission electron microscopy (cryoTEM). The method enabled the alignment of lipid nanotubes as an ensemble into various shapes with microfluidic systems.

In this work, we use the surface-assembled LNTs that we have reported previously[10] to demonstrate the "single" LNT patterning. In the previous work, the microfluidic systems controlled the orientation of the LNTs but not the number of the LNTs, which limited their applications. In the present approach, we use the pre-assembled LNTs or $H_{II}$ lipid blocks as a lipid reservoir from which new LNTs were pulled by applying a point load with a micromanipulator. The method allows for drawing any objects on substrates with a well-connected single LNT. Especially the LNT formation from $H_{II}$ lipid blocks just by micromanipulation is interesting, because the same simple approach does not work easily if the lipid reservoir is GUVs made of PC (phosphatidylcholine) lipids. We think that the property of the $H_{II}$ lipid reservoir is the key aspect, which allowed us the simplification of the patterning technique.

**Experimental Section**

*Buffer solution (HEPES buffer)*: All the experiments were performed in HEPES buffer solution at pH 7.4. The buffer solution was prepared with 10 mM 4-(2-hydroxyethyl)piperazine-1-ethanesulfonic acid (Fluka, Switzerland) and 0.15 M sodium chloride (Roth, Germany) in ultra-pure water filtered through MilliQ Gradient A10 filters (Millipore AG, Switzerland). The pH was adjusted to 7.4 using 4 M NaOH (Sigma–Aldrich Chemie GmbH, Switzerland).

*Polyelectrolytes and polyelectrolyte multilayers (PEMs)*: Polyethyleneimine (PEI, MW = 25,000 g/mol, branched, #408727), Poly(sodium 4-styrenesulfonate) (PSS) 30 % solution (MW ~ 70,000 g/mol, #527483) and Poly-L-lysine (PLL) 0.01 % solution (MW = 70,000 – 150,000, #P4707) were purchased from Sigma–Aldrich Chemie GmbH (Switzerland). PEI and PSS were dissolved or diluted at a concentration of 1 mg/ml in HEPES buffer solution. All the solutions were sterile filtrated through 0.22 $\mu$m filters. For single PEI coating, an oxygen-plasma-treated glass coverslip was incubated in PEI solution for at least 15 min before rinse. To form PEMs, an oxygen-plasma-treated glass coverslip was incubated in PEI and PSS solution alternately for 1 min each with rinse (HEPES buffer) in between. Such quick incubation allows us to save time and produces PEMs with a slightly reduced thickness than the ones incubated till adsorption saturation for each layer. Only for the last layer, PEI solution was incubated for at least 15 min before rinse to assure the good surface coverage.

*Mother lipid nanotube assembly:* The detail is described elsewhere.[10] In brief, 1,2-dioleoyl-sn-glycero-3-phosphoethanolamine (DOPE, #850725) and 1,2-dioleoyl-*sn*-glycero-3-phosphoethanolamine-N-(lissaminerhodamine B sulfonyl) (Liss Rhodamine-PE, #810150) were purchased from Avanti Polar Lipids and stored in chloroform. The lipid solution was prepared by taking DOPE + 0.5 % Liss Rhodamine-PE into a flask, drying and adding HEPES buffer solution, followed by sonication at the final concentration of 1 mg/ml. Upon sonication, lipids detach from the flask wall and form blocks of $H_{II}$ phase. The DOPE blocks were adsorbed onto the PEI-functionalized surface. A turbulent flow was given by a pipette to create random LNT networks followed by rinse.

*Transport experiment in Figure 1:* GUVs were formed by electroformation on ITO-coated glass slides as described elsewhere.[16] We used 1,2-dioleoyl-*sn*-glycero-3-phosphocholine (DOPC, #850375, Avanti Polar Lipids) dissolved in chloroform at 25 mg/ml for lipids and

300 mM sucrose solution for the hydration of the lipids. An AC voltage (10 Hz, 2 V/mm) was applied for 2 h. Caged-FITC (#F7103, life technologies) was dissolved in de-ionized water at 10 mg/ml as a stock solution. Caged-FITC has no fluorescence unless it is uncaged by UV. It was added to the GUV solution at the final concentration of 100 μg/ml and incubated at 40 C° for 2 h. The elevated temperature induces defect formation in GUVs, allowing the caged-FITC to go inside of the GUVs. Next, 100 μl caged-FITC-encapsulated-GUV solution was added on top of pre-patterned LNTs. Although GUVs sit on the surface-assembled LNTs, spontaneous fusion did not occur at high probability. Therefore, we placed a PLL-g-PEG-coated cover slip (#PLL(20)-g[3.5]-PEG(2), Susos AG, Switzerland) on top of the sample and applied a force manually (see the following schematic). LNTs and GUVs were squeezed in between two glass slips, and the mechanical force induced fusion in some places of the sample (typically GUVs are broken down into smaller sizes). PLL-g-PEG coating minimized the interaction between the top coverslips and lipids.

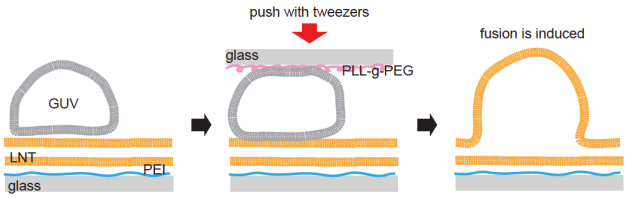


Local uncaging of FITC was performed by illuminating the center of a GUV by UV (typically 5 – 50 ms) with a confocal laser scanning microscope (CLSM). The transport of FITC via LNT was subsequently monitored also with CLSM.

*Sample chambers:* The sample consists of a donut-shaped PDMS block and a glass coverslip cleaned by an oxygen-plasma cleaner (100 Plasma System, PVA TePla, Germany) just before the experiments. PDMS blocks adhere to the glass surface acting as a wall to confine liquid inside.

*Fluorescent microscope setup:* Movies, from which snapshots were taken for figures, were recorded by Axiovert 200M (Zeiss, Germany) with an oil immersion objective (Objective Plan-Apochromat 63x/1.40 Oil DIC, Zeiss, Germany) for Figure 2-5, S1, S2, S4 and with LD Plan-Neofluar 40x/0.6 Corr Ph2 M27 (Zeiss, Germany) for Figure 6A. The contrast and the brightness were adjusted and the images were presented with false colors for figures.

*Micromanipulation:* Micromanipulator InjectMan NI 2 and micro-glass capillaries (FemtoTip II) were both purchased from Eppendorf, Germany. Although the system is made for microinjection, we only used it as a micromanipulator.

*Confocal laser scanning microscope (CLSM) and fluorescence recovery after photobleaching (FRAP)*: For Figure 1 and Figure S3 we used TCS SP5 CLSM (Leica, Germany) equipped with a white light laser, a UV laser and an oil immersion objective (HCX PL APO 63x/1.40-0.60).

*Histogram analysis;* The histogram in Figure 3 was produced with data from 5 movies (5 mother and daughter LNT couples) with the total duration of 32 s. Image J was used for the analysis.

*Atomic Force Microscopy (AFM)*: We used the Nanowizard II (JPK Instruments, Germany) and the Mikromasch CSC38/noAl cantilevers in the intermittent mode in fluid. For the scratch method, we scratched the surface of the PEMs with the backside of a razor blade and the trace of the scratch was imaged with AFM.

## Results and discussion

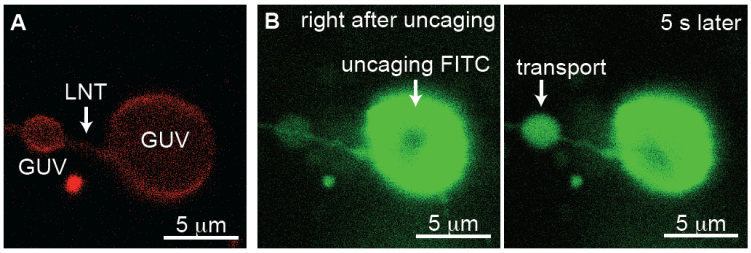


**Figure 1:** Two GUVs were mechanically connected with a LNT by pressing the GUVs against it. **A**, LNTs are labeled with Liss Rhodamine-PE. Upon fusion between the GUVs and the LNT, the Liss Rhodamine-PE diffused into the GUVs, staining the membrane of both GUVs red. **B**, Local uncaged FITC traveled from the right to the left GUV through the single LNT.

First, using the LNTs we show the transport of water-soluble dyes between two GUVs connected by a LNT. It demonstrates the possible use of the LNTs as a nano-biochannel, which motivates the main work in this manuscript. LNTs were pushed into contact with GUVs (see Experimental Section). LNTs are labeled with Liss Rhodamine-PE throughout this work. Upon fusion between the GUVs and the LNTs, the Liss Rhodamine-PE diffused into the GUVs and stained the GUV membrane red (Figure 1A). This shows that the lipid exchange from the LNT to the GUVs appears directly after they have been mechanically connected, implying the lateral connection of the membrane between the LNT and the GUV. Then, we observed the transport of FITC from the right to the left GUV (Figure 1B) by locally uncaging FITC with UV light within the right GUV only (for details refer to Experimental Section). Within less than 5 sec after uncaging caged-FITC, fluorescent dyes diffused from the right to the left GUV and increased the fluorescent intensity. Although the change in intensity is clearly visible, a change in volume between the two GUVs could not be detected probably because the both osmotic pressure and surface tension difference between those two GUVs were not large enough. These results give important information: (i) LNTs have the ability to fuse with GUVs, (ii) water-soluble material is exchanged between the GUVs. Thus, such a LNT-GUV network can be used as *e.g.* molecular/ionic circuits. Eukaryotic cells and bacteria also form similar tubes between their cell bodies to transport

intercellular organelles[17, 18] and to transmit electrical signals.[19] In this context, our synthetic LNTs may be also used to mimic biological tube structures between eukaryotic cells, opening interesting applications.

For such applications, the full control over the individual LNT positioning is critical. The main work of this manuscript describes a method to pattern "single" LNTs with the previously reported surface-assembled LNTs[10] (we call them mother LNTs in this work. A representative fluorescent image is shown in Figure S1) and a micropipette connected to a commercial micromanipulator.

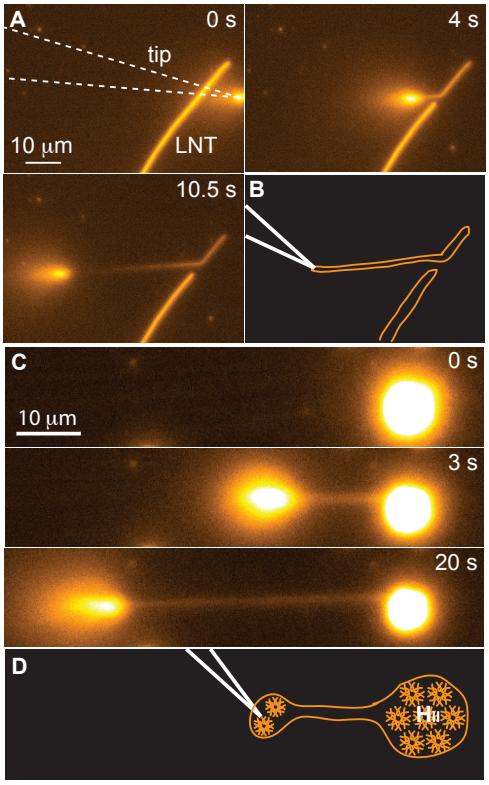


**Figure 2**: Daughter LNT formation with a pipette. With the tip of a glass micropipette a daughter LNT is pulled from **(A)** a mother LNT (snapshots from Movie S1) or **(C)** from a $H_{II}$ lipid block (snapshots from Movie S2). **A, C,** A sequence of fluorescent micrographs. **B, D,** Corresponding schematic images (micropipette shown in white).

When a micropipette physically crosses the mother LNT, a part of the mother LNT attaches to the glass micropipette (Figure 2A). The hydrophilic head group of DOPE lipids is favorable to the adhesion to the glass surfaces, which helps with the attachment. Subsequently, the micropipette applies a point load to the mother LNT, pulling out another

tube (Figure 2AB, Movie S1). The phenomenon resembles the nucleation of new LNTs from surface-patterned LNTs when mammalian cells made a point contact to the mother LNTs via focal contacts and pulled out daughter LNTs by acto-myosin mediated contractility.[20] The daughter LNTs are similarly formed from lipid blocks (Figure 2CD, Movie S2). This simple phenomenon is a critical difference from the interaction between a micropipette and a GUV. LNTs are commonly formed by applying a point load on GUVs by a micropipette[9] or by optical tweezers.[21] However, these approaches require additional tricks such as voltage pulse application or incorporation of biotin in the GUVs and coating of the pipette with streptavidin to assure the reproducible connection between the GUVs and the pipette. It is because GUVs do not adhere to the pipette otherwise, but rather try to dodge when one attempts to touch. In the present work, the $H_{II}$ lipid blocks made of DOPE simply attach to the glass pipette, and a new daughter LNT can be pulled out from the reservoirs. This is a large improvement in terms of the technical simplification, which surprisingly originates from the slight difference in the lipid properties between PC lipids that form lamellar GUVs and DOPE lipids that form $H_{II}$ phase. It is interesting since the efforts for LTN patterning have mainly focused on the development of new tools (voltage shock application,[9] micropipette aspiration[5] *etc*.) but not on the alternation of the type of lipids. In the following, we attempt to understand why LNTs form simply with a glass pipette without any special trick only from $H_{II}$ blocks unlike in the case with GUVs.

First, we begin with a comparison of forces involved in the tube formation. The initial force needed to create the neck between a flat bilayer and a tube pulled by a point load (commonly referred as overshoot force) is predicted as $f_{over} = 1.13 f_0$ where $f_0$ is the force for keep pulling the tube once the neck has formed.[22] Since $f_{over} > f_0$, the force vs tube length curve shows a characteristic overshoot followed by a constant force $f_0$ well-characterized both theoretically[22] and experimentally.[21, 23] The constant force is known as $f_0^{GUV} \approx 5$ - 15 pN for

the tube formation from GUVs[21-23] and $f_0^{HII} \approx 86$ pN for the one from $H_{II}$ blocks.[10] Since $f_0^{HII} > f_0^{GUV}$, the involved forces do not explain why the tube formation from the $H_{II}$ structure is more likely to happen. In any case, the micromanipulator can apply a much larger force than pN anyway, thus the force is not the limiting factor for the tube formation as long as the lipids attach to the pipette firmly. Interestingly, the overshoot force $f_{over}$ is larger if the pipette-GUV contact area $S$ is larger. By assuming the contact area is a flat circle with a radius of $R_{contact}$ ($S = \pi R_{contact}^2$), the relation follows $f_{over} / f_0 = 1 + 0.5\ R_{contact}/R_{tube}$ in the large $R_{contact}$ range, where $R_{tube}$ is the tube radius.[21] Nevertheless, to create a large contact area between the reservoir and the pipette probably has an advantage for pulling a tube since the adhesion energy is proportional to the adhesion area $S$ ($= \pi R_{contact}^2$) while $f_{over}$ is to the radius $R_{contact}$. When we consider a large contact area (> 1 $\mu m^2$) at the tip of a micropipette (typically the opening diameter is 200 – 400 nm), the assumption that the contact area is a flat circle is not valid anymore. The tip of the pipette is rather a cylinder and the coverage of the cylindrical surface with a lipid bilayer by deforming a GUV has an extremely large energy penalty as studied in detail.[24] It explains why poking a GUV with a pipette does not result in a large coverage of the pipette tip with the bilayer. On the other hand, contacting a $H_{II}$ block with a pipette can end up with a coverage of the pipette tip with the lipids. In fact, even the fission of $H_{II}$ blocks can be performed simply by squeezing a $H_{II}$ block between a substrate and a pipette tip, which often results in adsorption of a part of the block to the pipette tip while the counterpart remains adhered to the substrate, spanning a tube in between when the pipette is moved away from the lipid block (Figure 2C). It leads us to think that the characteristic of $H_{II}$ blocks to be able to flexibly deform and adhere to a pipette with a large contact area may be a key feature, which helps to create a firm connection between the pipette and the lipid reservoir and increases a chance to withstand the overshoot force $f_{over}$ when the pipette is retracted to form a tube.

In this perspective, next we discuss the deformation of GUVs and $H_{II}$ blocks. We suppose that the deformation of GUVs is accompanied by a change in the surface area, while the internal volume is kept constant. This assumption is experimentally true shown by micropipette aspiration (unless an extremely high-pressure aspiration is applied over hours) thus commonly used for theoretical works.[25] The deformation of GUVs increases the free energy of the system by the bending energy and the surface tension (the energy required to increase the unit surface area). The bending energy can be estimated with the bending modulus of PC lipids ($\kappa_{GUV} \approx 40$ - 90 pNnm)[25] and the shape of the deformation.[24] The surface tension $\sigma$ is more cumbersome since it is not a constant value. We define the increase rate of the surface area as $\Delta\alpha/\alpha_0$ (where $\alpha_0$ is the apparent surface area of a GUV before the deformation and $\Delta\alpha$ is the change in the apparent surface area of the GUV upon the deformation).[25] In the high-tension regime ($\Delta\alpha/\alpha_0 > 0.01$), the area expansion is performed by a direct stretch of the membrane. Therefore, $\sigma$ is a function of $\Delta\alpha/\alpha_0$, rapidly increases as $\Delta\alpha/\alpha_0$ increases and can reach up to $\approx$ 13 pN/nm before the GUV breaks.[26] On the other hand, $H_{II}$ lipid block is a lipid bilayer envelope packed with lipids in $H_{II}$ phase as we and other researchers have previously reported with cryoTEM images.[10, 14] When the block is deformed, the internal $H_{II}$ structure does not change the free energy before and after the deformation since they are in the same phase. At the surface, the outer most bilayer induces a bending energy similarly to the case of GUVs. Considering that the bending modulus $\kappa$ of PC lipids and that of DOPE ($\approx$ 90 pNnm)[27, 28] are roughly the same, there is little difference in the bending energy between these two systems under the same deformation. Therefore, next we focus on the surface tension. The deformation of a $H_{II}$ block also increases the surface area. However, it is not achieved by stretching the bilayer as in the case of GUVs but by transferring the material form the internal $H_{II}$ structure to the surface lamellar bilayer to

supplement the lipids that are needed for making the additional bilayer area. Therefore $\sigma_{HII}$ originates from the energy cost to transform lipids from $H_{II}$ phase to L (lamellar) phase. According to the previous theoretical studies on DOPE,[10, 29] the total free energy of a number of lipids $N = 2A/a$ ($a \approx 0.65$ nm$^2$ is the area per lipid molecule,[29] $A$ is the bilayer area) can be described as

$$E_{\mathrm{H}} = \varepsilon_i A \tag{1}$$

$$E_{\mathrm{L}} = \left\{\frac{\kappa}{2}\left(\frac{1}{R_0}\right)^2 - W\right\} A \tag{2}$$

for the $H_{II}$ phase and the L phase, respectively. The free energy of the $H_{II}$ phase ($E_H$) contains no elastic term (zero bending energy) because the lipid monolayers take the radius of the spontaneous curvature ($R_0 \approx 2.85$ nm)[27, 29] in fully hydrated $H_{II}$ phase. $\varepsilon_i$ is the energy density of the interstitial energy ($\varepsilon_i = 2g_i/a \approx 4.5$ pN/nm,[29] where $g_i$ is the interstitial energy per lipid molecule) which originates from the voids in the hexagonal interstices. The free energy of the L phase ($E_L$) consists of the elastic energy of a flat bilayer (with a bending modulus $\kappa \approx 90$ pNnm)[27, 28] and the second term (with energy density $W \approx 0.1$ pN/nm)[29] that comprises all the interactions between the bilayers (including Van der Waal attraction and hydration repulsion). The energy cost $\Delta E$ for the phase transformation from $H_{II}$ to L per bilayer area is

$$\frac{\Delta E}{A} = \frac{E_L - E_{\mathrm{H}}}{A} = \frac{\kappa}{2}\left(\frac{1}{R_0}\right)^2 - W - \varepsilon_i$$

$$= (5.5 - 0.1 - 4.5)\ \text{pN/nm} \tag{3}$$

$$= 0.9\ \text{pN/nm} = \sigma_{\text{HII}}$$

From the comparison of the value of each term (the second line in Equation (3)), we see that the system is fundamentally a competition between the bending energy and the interstitial energy $\varepsilon_i$ ($W$ is negligible). The value $\sigma_{\text{HII}}$ = 0.9 pN/nm is more than one order of magnitude smaller than that of GUVs ($\sigma_{\text{GUV}} \approx 13$ pN/nm at a large deformation). Importantly, $\sigma_{\text{HII}}$ is a constant value and is independent of the apparent area expansion $\Delta\alpha/\alpha_0$, while $\sigma_{\text{GUV}}$ keeps increasing as $\Delta\alpha/\alpha_0$ increases. It shows that the large deformation ($\Delta\alpha/\alpha_0 > 0.01$) of GUVs is extremely difficult because the more they deform the higher $\sigma_{\text{GUV}}$ becomes since $\sigma_{\text{GUV}}$ originates from stretching the bilayer. On comparison, the deformation of $H_{II}$ blocks in the same $\Delta\alpha/\alpha_0$ regime is easier because $\sigma_{\text{HII}}$ is a constant value thanks to the internal reservoir that keeps supplying the lipids. It could partially explain why we can deform $H_{II}$ blocks so easily compared to GUVs. Besides, the internal $H_{II}$ structure may have acted as a scaffold to prevent the bock from dodging when being poked. Both contribute to have a large contact area with a curved object such as pipettes upon contact. It is an advantage for forming a firm adhesion to the pipette, thus for pulling a tube. In addition, the adhesion energy between the glass pipette and the lipids can be slightly different depending on the lipid type (PC or PE) even though both are zwitterionic lipids. It may have also affected the pipette-lipid interactions.

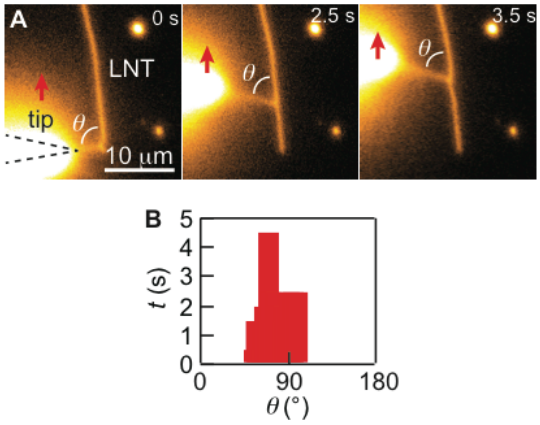


**Figure 3: A,** A daughter LNT slides along a mother LNT (snapshots from Movie S3). **B,** The histogram shows the angle ($\theta$) between the mother and daughter LNT. The histogram is based on data from 5 individual movies (i.e. 5 mother and daughter LNT couples) with a total duration of 32 s.

By increasing the height of the micropipette right after crossing the mother LNT, one can prevent the daughter LNT from touching the substrate. This produces a free-hanging LNT between the pipette and the mother LNT. Such spanned daughter LNTs slide along the mother LNTs when the micropipette is moved in parallel to the mother LNTs (Figure 3, Movie S3). Interestingly, the daughter LNTs move while maintaining the angle between the mother and the daughter LNT $\theta$ at around 90°. This can be explained because the perpendicular angle between the mother and the daughter LNT causes minimal surface tension based on the theory we have previously constructed for the LNT assembly.[10]

The daughter LNT remains free-hanging between the micropipette and the lipid block (or mother LNTs) unless the micropipette is moved upwards fast to rip off the tube. Whereas if the pipette is lowered onto the surface, the daughter LNTs occasionally adhere to the substrate. However, the anchoring probability and the position of the anchor points were not reproducible enough to draw complex objects. It may be because the contact between the micropipette and daughter LNTs is not right at the tip but slightly away from the aperture of the pipette. In this case, bringing down the pipette onto the surface does not promote direct contact between the substrate and the LNT and anchoring fails.

Alternatively, we found a reliable method to anchor the daughter LNTs on the surface of a polyelectrolyte multilayer (PEM). Polyelectrolytes, such as PEI, which we use as a starting surface to form LNTs, are charged polymers that can be assembled into multilayers by alternately depositing cationic and anionic polymers.[30] PEI is commonly used as an adhesion layer between substrates and PEMs. However, it has been rarely used in PEM matrixes. One of the rare systems that has been previously characterized is $(PEI/PSS)_n$ (PSS; Polystyrenesulfonate) where $n$ represents the number of the bilayers. Therefore, we prepared a PEM-coated glass coverslip with $(PEI/PSS)_{20}PEI$. The advantages of this platform are: First, the PEM increases the surface roughness which may improve the probability of LNT-surface contact. Second, it facilitates the assembly of mother LNTs since the top layer is PEI. We tested the formation of LNTs on the $(PEI/PSS)_nPEI$-coated glass surface at different bilayer numbers ($n$ = 5, 10, 15, 20). LNTs assembled on the PEMs independent of the bilayer number (Figure S2). We also attempted the formation of LNTs on a different PEM, $PEI/PSS(PLL/PSS)_{20}PEI$, where the top layer is also PEI. However, LNTs did not form in this case. It implies that the termination of PEMs with PEI is not the only condition for LNTs to form on PEMs.

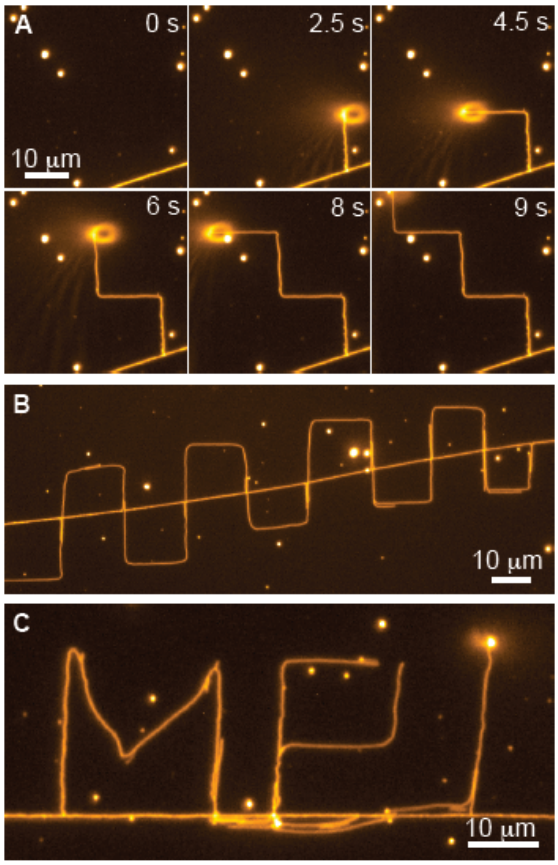


**Figure 4: A-C,** Examples of free drawing a single LNT (correspondig movies are available in Movie S4-6). The tip of the micropipettes can be recognized by the bright dot at the end of LNTs. All the figures were drawn in less than a few minutes. The created LNT objects were stable over 6 days (Figure S4).

Figure 4A-C shows the free drawing of single LNTs using the PEM-coated substrates (Movie S4-S6). The daughter LNTs were pulled from a mother LNT as described before. The micropipette was constantly kept in contact with the substrate and freely moved in the desired direction by the micromanipulator. The daughter LNTs followed the trace of the micropipette and stayed at the position even after the micropipette was removed from the surface. Compared to the drawing on the single PEI-coated glass surface, the overall controllability of the daughter LNT attachment was significantly improved. It allows for the patterning of single LNTs in any shape. Fluorescence recovery after photobleaching (FRAP) shows the fluidity of the daughter LNTs and the continuous connection to the mother LNTs (Figure S3). The FRAP data in Figure S3 and in our previous report[10] both suggest that the tube-tube

junctions are well-fused and connected. It implies that when two LNTs look crossing over in a fluorescence image, in many cases they are fused and formed a four-way junction instead of laying on top of each other. The created lipid structures were stable for at least six days (Figure S4).

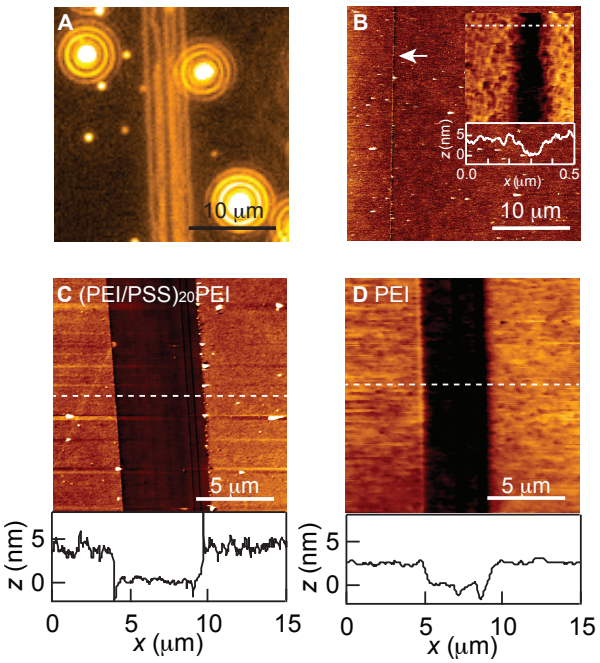


**Figure 5: A,** fluorescent image of daughter LNTs. **B,** AFM image of an area around A (not perfectly the same place but along the daughter LNTs). **C,** AFM image of a PEM with a scratch. **D,** AFM image of a single PEI layer with a scratch. The cross sections at the white dotted lines are shown below for both C and D.

To study why the PEM increased the controllability of the LNT anchoring, samples were imaged with atomic force microscope (AFM). Figure 5A shows a fluorescent image of Liss Rhodamine-PE-stained daughter LNTs drawn by moving the pipette in line once. Note, that micropipettes already contaminated by lipids frequently create several daughter LNTs at once. Figure 5B shows an AFM image taken along such surface-pattern daughter LNTs. A trace of a scratch (see the white arrow and the inset) corresponds to the movement of the pipette because the pipette removes the PEM material from the surface. From these images we can say that there is no colocalization between the daughter LNTs and the scratch. Note that the LNTs were impossible to image with AFM probably because they are extremely soft

and fluidic. Next, the thickness and the surface topology of the PEM were studied by scratching the polymer layers with the backside of a razor blade and imaging the trace with AFM. This gives a clearer profile than the scratch produced by the micropipette (the one in the inset in Figure 5B), allowing us to estimate the thickness more accurately (commonly called "scratch method").[31] The cross section of a scratch in Figure 5C implies a PEM thickness of approximately 5 nm and an increased surface roughness compared to the single PEI coating (compare Figure 5D). Previously, Elzieciak and coworkers have studied the assembly of $(PEI/PSS)_n$, combining ellipsometry, quartz crystal microbalance (QCM), AFM and cyclic voltammetry.[32] At the same pH condition as our experiment (pH = 10 for PEI solution, pH = 7.4 for PSS solution. Note that in our experiments even though PEI was dissolved in pH = 7.4 HEPES buffer, the PEI solution has pH 10 since the concentration of 1 mg/ml is out of buffering zone). The thickness from the ellipsometry showed a zig-zag trace as a function of $n$ with an extremely slow non-linear growth rate ($\approx$ 3 nm at $n$ = 6 with PEI as the top layer).[32] Their AFM images revealed that, rather than increasing the thickness, the layer-by-layer assembly increases the surface roughness by reshaping polymer droplets on the surface. In the article, the growth behavior was linked to the low protonation rate of PEI at pH = 10.5 (low charge density) and the removal of polymers from the surface during rinsing. Both, the thickness and the surface morphology obtained by our AFM images in Figure 5C correspond well to their previous report.

It is somewhat surprising that the change in the topology by a few nm dramatically altered the anchoring behavior of the daughter LNTs. As we discussed previously, the daughter LNTs may be attached not right at the tip of the pipette but slightly away from the aperture. If this distance is a few nm, the increase in surface roughness at the nanometer scale could increase the probability of LNT-surface contact. Other than the topology, the electric charge of the PEM surface may be different from PEI, although, the top layer is known to

mainly govern the total charge of the PEM. It may have also affected the adhesion behavior. Apart from $(PEI/PSS)_{20}PEI$, there may be other polyelectrolyte couples that also similarly improve the adhesion, although the fabrication of mother LNTs on top of the PEMs is rather a challenge as we discussed previously.

## Conclusion

We report a simple well-controlled approach to free-draw single LNT objects on surfaces. The main advantages are; i) the method requires a simple instrumental setup, a fluorescent microscope and a micromanipulator without the need for the voltage applications. ii) The second advantage is that lipid objects consist only of LNTs without using GUVs at each anchoring point since they are directly attached to the surface of PEMs. We studied the characteristic of the surface tension of $H_{II}$ blocks, and found that $H_{II}$ blocks have an internal lipid supply that keeps the surface tension constant at the low value $\sigma_{HII} = 0.9$ pN/nm over a large regime of deformation. It helps to partially explain why $H_{II}$ blocks deform easily when they are poked by a micropipette and are able to adsorb on to the curved surface at the tip of the pipette, which allows for pulling the tube easily. The created objects were stable for more than 6 days due to the solid substrate that supports and enhances the stability of the created lipid objects. The method can be applied to create nano-biochannels between GUVs/cells, molecular/nanoparticle patterning by attaching molecules to the LNTs, and for metal-nanowire circuit fabrication by metallization of the surface-drawn LNTs.

## Supporting information

Supporting figures (Figure S1 – S4), and Movies (Movie S1 – S6). The time scale of all the movies is x3.5.

**Acknowledgements**

KS gratefully acknowledges the support of the Swiss National Science Foundation (SNSF) and Alexander von Humboldt Foundation. Part of the research leading to these results has received funding from the ERC Advanced Grant No° 294852. This work is also part of the excellence cluster CellNetworks at the University of Heidelberg. J.P.S. has a Weston Visiting Professorship at the Weizmann Institute of Science. The Max Planck Society is highly acknowledged for its support.

## References


1. P. Yager and P. E. Schoen, *Molecular Crystals and Liquid Crystals*, 1984, **106**, 371-381.
2. K. Yamada, H. Ihara, T. Ide, T. Fukumoto and C. Hirayama, *Chem Lett*, 1984, 1713-1716.
3. N. Nakashima, S. Asakuma and T. Kunitake, *J. Am. Chem. Soc.*, 1985, **107**, 509-510.
4. J. M. Schnur, *Science*, 1993, **262**, 1669-1676.
5. H. Frusawa, A. Fukagawa, Y. Ikeda, J. Araki, K. Ito, G. John and T. Shimizu, *Angewandte Chemie International Edition*, 2003, **42**, 72-74.
6. P. Pascoal, D. Kosanic, M. Gjoni and H. Vogel, *Lab on a Chip*, 2010, **10**, 2235-2241.
7. C. Leduc, O. Campas, J. F. Joanny, J. Prost and P. Bassereau, *Bba-Biomembranes*, 2010, **1798**, 1418-1426.
8. J. J. Benkoski, A. Jesorka, M. Edvardsson and F. Hook, *Soft Matter*, 2006, **2**, 710-715.
9. A. Karlsson, R. Karlsson, M. Karlsson, A.-S. Cans, A. Stromberg, F. Ryttsen and O. Orwar, *Nature*, 2001, **409**, 150-152.
10. K. Sugihara, M. Chami, I. Derenyi, J. Voros and T. Zambelli, *ACS nano*, 2012, **6**, 6626-6632.
11. R. Koynova and M. Caffrey, *Chem. Phys. Lipids*, 1994, **69**, 1-34.
12. R. P. Rand and N. L. Fuller, *Biophys. J.*, 1994, **66**, 2127-2138.
13. E. Y. Shalaev and P. L. Steponkus, *Biochimica et Biophysica Acta (BBA) - Biomembranes*, 1999, **1419**, 229-247.
14. D. P. Siegel, W. J. Green and Y. Talmon, *Biophys. J.*, 1994, **66**, 402-414.
15. R. Van Venetië and A. J. Verkleij, *Biochimica et Biophysica Acta (BBA) - Biomembranes*, 1981, **645**, 262-269.
16. R. Dimova, S. Aranda, N. Bezlyepkina, V. Nikolov, K. A. Riske and R. Lipowsky, *J Phys-Condens Mat*, 2006, **18**, S1151-S1176.
17. A. Rustom, R. Saffrich, I. Markovic, P. Walther and H. H. Gerdes, *Science*, 2004, **303**, 1007-1010.
18. G. P. Dubey and S. Ben-Yehuda, *Cell*, 2011, **144**, 590-600.
19. X. Wang, M. L. Veruki, N. V. Bukoreshtliev, E. Hartveit and H. H. Gerdes, *Proc. Natl. Acad. Sci. U. S. A.*, 2010, **107**, 17194-17199.
20. K. Sugihara, M. Delai, R. Mahnna, J. Kusch, D. Poulikakos, J. Voros, T. Zambelli and A. Ferrari, *Integrative biology : quantitative biosciences from nano to macro*, 2013, **5**, 423-430.
21. G. Koster, A. Cacciuto, I. Derenyi, D. Frenkel and M. Dogterom, *Phys Rev Lett*, 2005, **94**.
22. I. Derényi, F. Jülicher and J. Prost, *Phys Rev Lett*, 2002, **88**, 238101.
23. D. Cuvelier, N. Chiaruttini, P. Bassereau and P. Nassoy, *Europhys Lett*, 2005, **71**, 1015-1021.
24. J. Z. Y. Chen and S. Mkrtchyan, *Phys Rev E*, 2010, **81**.
25. W. Rawicz, K. C. Olbrich, T. McIntosh, D. Needham and E. Evans, *Biophys. J.*, 2000, **79**, 328-339.
26. D. Needham and R. S. Nunn, *Biophys. J.*, 1990, **58**, 997-1009.
27. Z. Chen and R. P. Rand, *Biophys. J.*, 1997, **73**, 267-276.
28. S. Leikin, M. M. Kozlov, N. L. Fuller and R. P. Rand, *Biophys. J.*, 1996, **71**, 2623-2632.
29. M. M. Kozlov, S. Leikin and R. P. Rand, *Biophys. J.*, 1994, **67**, 1603-1611.
30. G. Decher, *Science*, 1997, **277**, 1232-1237.

31. K. Sugihara, J. n. Vörös and T. Zambelli, *The Journal of Physical Chemistry B*, 2010, **114**, 13982-13987.
32. A. Elzieciak, S. Zapotoczny, P. Nowak, R. Krastev, M. Nowakowska and P. Warszynski, *Langmuir*, 2009, **25**, 3255-3259.

We developed a simple well-controlled approach to free-draw single lipid nanotube (LNT) objects on surfaces.